Silicon Photomultipliers With Area Up to 9 mm² in a 0.35-μm CMOS Process

**XIAO LIANG[1], NICOLA D'ASCENZO [1,2,3] (Member, IEEE), WERNER BROCKHERDE [4] (Member, IEEE),
STEFAN DREINER[4], ANDREI SCHMIDT [4], AND QINGGUO XIE[1,2,3] (Member, IEEE)**

1 School of Life Science and Technology, Huazhong University of Science and Technology, Wuhan 430074, China
2 Wuhan Laboratory of Optoelectronics, Wuhan 430074, China
3 Istituto Neurologico Mediterraneo, Neuromed I.R.C.C.S., 86077 Pozzilli, Italy
4 Fraunhofer Institute for Microelectronics Circuits and Systems IMS, 47057 Duisburg, Germany

CORRESPONDING AUTHORS: N. D'ASCENZO, W. BROCKHERDE, AND Q. XIE (e-mail: ndasc@hust.edu.cn; werner.brockherde@ims.fraunhofer.de; qgxie@hust.edu.cn)

ABSTRACT Silicon photomultipliers produced using standard complementary metal oxide semiconductor (CMOS) processes are at the basis of modern applications of sensors for weak photon fluxes. They allow in fact to integrate transistor-based electronic components within sensors and provide intelligent read-out strategies. In this paper, we investigate the scalability of a 0.35-μm CMOS process to large area devices. We report the design and characterization of SiPMs with a total area of 1, 4, and 9 mm². Cross talk, photon detection efficiency at 420 nm, gain at 2.5 V overvoltage and breakdown voltage temperature coefficient do not depend on the total area of the sensor and are 10%, 35%, 2.5×10^6, and 35 mV/K, respectively. The dark count rate scales with the total area of the device as 180 kHz/mm². The total output capacitance, the decay time of the single photon signal, and the single photon time resolution depend on the area of the device. We obtain a capacitance of 66.9, 270.2, and 554.0 pF, a decay time of (27.1 ± 0.1) ns, (50.8 ± 0.1) ns, and (78.2 ± 0.1) ns and a single photon time resolution of (77.97 ± 0.51) ps, (201.67 ± 0.98) ps, and (282.28 ± 0.86) ps for the 1, 4, and 9 mm² SiPMs, respectively.

INDEX TERMS Silicon photomultiplier (SiPM), avalanche breakdown structures, CMOS, sensors for brain positron emission tomography.

I. INTRODUCTION

The silicon photomultiplier (SiPM) is a silicon sensor suitable to the detection of weak fluxes down to few photons/mm². It is composed of an array of microcells with internal gain of approximately 10^6 electrons per detected photon under a typical bias of few tens of Volts. Each microcell has a size ranging between 20 μm and 100 μm, is operated in non-proportional mode and produces a signal when a photon is detected. The parallel array of microcells outputs a signal proportional to the photon flux. The SiPM is rapidly substituting photomultiplier tubes in a wide range of applications, for instance in high energy physics, medical equipment, astrophysics and homeland security. A stable production of the SiPMs is currently available at few leading manufacturers [1]–[5]. The commercial

SiPM exhibits, among others, a dark count rate as low as $80 - 100$ kHz/mm² [2], a gain up to 6×10^6 at an overvoltage of 2.5 V [2], a photon detection efficiency up to 30%-40% at a wavelength in the range between 400 nm and 420 nm [5], and a single photon time resolution (SPTR) of approximately 100 ps [3].

However, modern applications of photon detectors, such as Light Detection and Ranging (LIDAR) systems, quantum imaging and quantum communication, require a fast processing of the signals corresponding to a given photon detection pattern. Time to digital converters (TDC), inverters, digital memories and other transistor-based electronic components are thus integrated within the sensing elements [6]–[9]. The problem here is that commercially available SiPMs are obtained in custom processes, while the

inclusion of electronic components in the chip is possible only using the standard implantations offered by complementary metal oxide semiconductor (CMOS) processes. The challenge of the design of modern SiPMs is thus to fabricate single photon sensing structures using standard CMOS processes and to reach performances comparable to commercial devices obtained with custom technology. For example, the sensor layers of the Sensl-C SiPM were imported in a 0.35 μm CMOS node. The process was used to fabricate a SiPM test chip composed of 7×7 micro-cells with size 35 μm^2 including an on-chip amplifier. The device exhibited approximately 38% photon detection efficiency at 5 V overvoltage and 65 ns recovery time [10].

Several tests of SiPM and SiPM-like detection structures were reported in the literature using 0.8 μm [11]–[19], 0.7 μm [20], 0.5 μm [21], [22], 0.35 μm [23]–[34], 0.18 μm [6], [35]–[38], 0.15 μm [39], 0.13 μm [40]–[45], 0.09 μm [46], [47] CMOS processes. Avalanche diode structures compatible with standard nanometer scale CMOS technology [48] and based on SiGe [49] are also being studied.

A limit of the reported results is the absence of data regarding the scalability of the CMOS production process to large area SiPMs. On the one hand, the larger is the SiPM area, the larger is the number of hot pixels with a consequent increase of the dark rate. On the other hand, the output capacitance between the cathode and the substrate increases with the sensor area with a consequent deterioration of the output signal. This is a limiting factor to achieve a good signal to noise ratio in large area SiPMs. Commercial SiPMs obtained with custom technology are available with an area up to 36 mm^2 [3]. The technology scalability to a larger area is thus needed to establish a reliable comparison between SiPMs obtained with CMOS process integration and custom technology.

CMOS SiPM prototypes with area up to 1 mm^2 are reported in the literature. For example, a 1.1×1.1 mm^2 SiPM prototype composed of 242 microcells was produced using a 0.8 μm CMOS process. The active quenching circuit chosen in the SiPM operation reduced the output capacitance to 5.6 pF/mm^2 but the dark count rate at room temperature was as high as 3 MHz/mm^2 [18]. A 1.7×1 mm^2 SiPM prototype composed of 400 microcells with 50 μm pitch was produced using a 0.35 μm CMOS process. The integrated amplifier for each column of pixels allowed to reduce the output capacitance to 1.1 pF with a minimal impact on the filling factor. The dark rate was reduced to 1 MHz/mm^2 at 2.5 V over-voltage [53]. CMOS SiPMs prototypes with area larger than about 1 mm^2 are not reported in the literature up to our knowledge. We have recently presented a 1 mm^2 SiPM developed with a 0.35 μm CMOS process [34]. The device was composed of 20×20 microcells with size 50×50 μm^2. The device exhibited 200 kHz/mm^2 dark count rate, 10% cross talk probability, 1.5% afterpulsing probability, 5.35×10^6 intrinsic gain and 30% photon
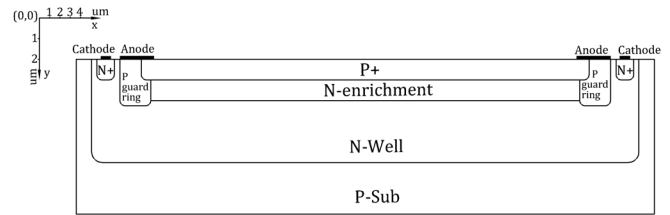
FIGURE 1. Cross section of the fabricated SiPM in 0.35 μm CMOS node [34]. The scale in micrometers is shown on the upper left corner in order to quantify the physical size of each layer. The length (x) and the depth (z) of the layers are identical. The n$^+$ contact has a square shape with size 1.8 $\times$ 1.8 μm^2.

detection efficiency for 420 nm wavelength at 29 V operational voltage. Although these results demonstrated that the used CMOS process offers a good platform for the development of a CMOS SiPM, the investigation of the scalability to devices with larger area was not reported.

In this paper we investigate the scalability of the 0.35 μm CMOS technology used in [34] to SiPMs with area up to 9 mm^2. We produced 120 SiPMs with area 1 mm^2, 4 mm^2 and 9 mm^2 using a standard 0.35 μm CMOS process and we characterized the devices both in dark and in illumination condition. We analyze the scalability of dark current, dark count rate, cross talk, single photon signal shape and single photon time resolution with the area of the device and we demonstrate that the obtained CMOS SiPMs with area up to 9 mm^2 are suitable for the detection of low photon flux.

II. MATERIALS AND METHODS
A. DEVICE FABRICATION
The 0.35 μm technology process used in this paper is an advanced mixed-signals CMOS process providing 4 metal layers, two polysilicon layers, high resistance polysilicon and two types of transistor gates (3.3 V and 5 V). The SPAD Implantation and the UV transparent passivation are special process options of the technology.

The design follows the guidelines already presented in [35]. The cross-section of a sensitive cell of the SiPM is shown on Fig. 1. A p$^+$/nwell junction is obtained with a n-enrichment implantation in the standard CMOS n-well. Light-doped p-type guard rings are used to prevent localized breakdown at the edges of the diode. The size of a sensitive cell is 50×50 μm^2. We developed three SiPMs prototypes with area 1 mm^2, 4 mm^2 and 9 mm^2 and number of cells 20×20, 40×40 and 60×60 respectively. The cells have common anode and cathode within a common n-well realized in a p-doped substrate.

When a photon or a thermally generated electron initiates an avalanche in one of the sensitive cells, a quenching mechanism is needed. We use a 220 kΩ passive quenching resistor realized with a high resistance polysilicon process. The resistor is integrated at the corner of each sensitive cell and has a width and length of 1 μm and 58 μm, respectively.
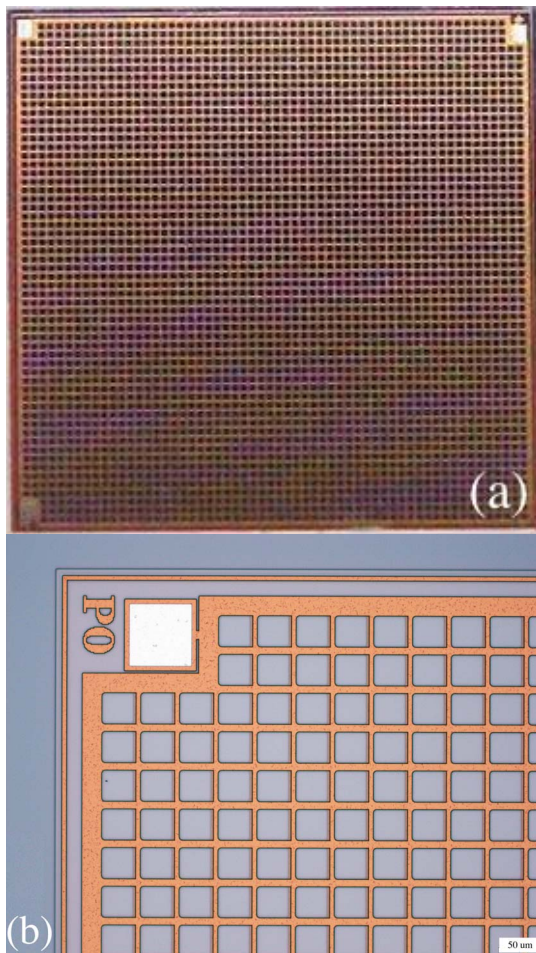
FIGURE 2. Chip view of the 9 mm^2 SiPM produced at the 0.35 μm CMOS node and (a) and zoomed view in the upper corner of the device (b).

The devices were produced in a dedicated engineering run. A chip view of the 9 mm^2 and a zoomed view in the upper corner of the device are shown in Fig. 2. A wafer hosts 124 identical dices with area 19700×9260 μm^2. We produced 10 wafers. The results presented in this paper include the average characterization of 120 devices selected across dices and wafers randomly.

B. CURRENT-VOLTAGE CHARACTERIZATION

A Keithley 2636 source meter, connected to a computer, obtained measurements of the current in reverse mode at wafer level and at room temperature. The measurement was performed in a optically isolated container. The supplied voltage was swept between 15 V and 32 V with 0.1 V steps and the corresponding current for each bias was measured. The upper limit of the current was set to 20 mA in order not to damage the device.

A dedicated setup was used to study the dependence of the current-voltage curve on the temperature. The SiPM was placed in a optically and thermally isolated container, whose temperature was set by a temperature controller (LAKESHORE 325). A vacuum electromagnetic valve

(GDC-J25) controlled the flow of nitrogen used to cool the system and connected the two terminals of the SiPM to the semiconductor analyzer (AGILENT B1500A). The current-voltage characteristics of the SiPM was measured at a reverse voltage range between 15 V and 32 V, with 10 mV steps, and in a temperature range between 253 K and 313 K, with 5 K steps.

A digital derivative of the current-voltage curve was calculated with a first-order simple numerical scheme. The two points of maximal derivative corresponded to the breakdown voltage V_{br} and the punch voltage between the space charge regions of the upper main (p+/nwell) and lower secondary (n-well/p-substrate). The measurement at a bias voltage $V_{br} - 0.1$ V was used to estimate the dark current in the proportional response region before breakdown.

The output capacitance was measured using a multifrequency capacitance-voltage meter (KEITHLEY PCT-CVU) at 10 kHz and at a bias $V_{br} - 0.05$ V.

C. DARK COUNT RATE AND CROSS TALK

The SiPM was placed in a light tight box. The SiPM was biased with a negative voltage applied to the anode, while the cathode was connected to ground. The signal was collected from the cathode on a 50 Ω load resistor and amplified of a factor 10 with a voltage wideband amplifier [58]. The SiPM was soldered on the amplifier board in order to remove the pick-up noise typical of high frequency fast amplifiers. The signal was sent to a threshold discriminator (CAEN N844). The number of pulses below threshold was registered within a 1 s observation time window. A threshold scan with 1 mV pitch was performed up to the amplitude corresponding to approximately 3 photoelectrons.

The dark count rate follows a series of plateaux with decreasing population when increasing the voltage threshold. The first one corresponds to the level of electronic noise, the second one to a single dark rate pulse due to thermal excitation, the nth one to n-1 coincident pulses from independent cells within the observation time window. The dark count rate of the SiPM was estimated at the voltage threshold with an amplitude of half a single pulse, which corresponds to the level of the first observed plateaux.

The optical and electrical cross talk was estimated as the ratio of the amplitudes of the first and second plateaux population, following [51].

D. GAIN

We illuminated the device by using a 550 nm LED, driven by a Keysight 81133A pulse pattern generator, with a pulse width of 10 ns. The light pulses were delivered to the operation position in the light protected area by an optical fiber. The SiPM and the light source were kept at a relative distance of 1 cm, with an alignment precision of 0.1 mm. The system was tuned to provide a small number of detected photons. The SiPM was biased with a negative voltage applied to the anode, while the cathode was connected to ground. The signal was collected from the cathode on a 50 Ω load

resistor and amplified of a factor 10 with a voltage amplifier [58]. The charge of the signal was measured within an integration gate of 100 ns using the CAEN V1180 QDC VME module.

The histogram of the measured charge consists of a series of peaks correspondent to the number of detected photons. The first peak corresponds to 0 detected photons (electronic noise pedestal), the second one corresponds to 1 detected photon, the $(n + 1)^{th}$ one to n detected photons. The gain was estimated as the average distance of the peaks divided by the gain of the amplifier and the charge of an electron.

E. PHOTON DETECTION EFFICIENCY
Following the method proposed in [51] and used in [34], we measured first the quantum efficiency (QE), including the avalanche probability, of a single sensitive cell produced on the same silicon wafer. Subsequently, the effective PDE of the SiPM was directly estimated by multiplying the QE of a single sensitive cell by the filling factor of the SiPM. The sensor was biased at an overvoltage of 2.3 V. The QE of a single sensitive cell was measured at wavelengths in the visible and near infrared. The measurement setup consisted of a monochromator, a Ulbricht sphere and lenses to focus the illumination on the active area of the device under test. A beam splitter and a calibrated photodiode at the monochromator output facilitated reference irradiance measurements while simultaneously recording the photocurrent of the device under test. The PDE of the SiPM was obtained by rescaling the QE of a single microcell by the geometrical filling factor, which was estimated from the layout as approximately 68% for all the fabricated devices.

F. SINGLE PHOTON TIME RESOLUTION
The SiPM was placed in an optically isolated container and was illuminated with a picosecond fast pulsed diode laser emitting light at a wavelength of 440 nm (PICOQUANT LDH-P-C-440). The laser diode was driven by the pulsed diode laser driver (PICOQUANT PDL 800-B) at a frequency of 2.5 MHz. The laser head was placed at a distance of 20 cm from the SiPM. The voltage amplitude of the driver and the corresponding emission power is kept at the suggested values by the producer in order to guarantee a fast light pulse with 50 ps (FWHM). The light flux at the surface of the SiPM was reduced to few photons/mm^2 and was made uniform using respectively a series of $10\times$ and $10^6\times$ filters (THORLABS NE10A and NE60A) and a round 20 degree circle tophat diffuser (THORLABS ED1-C20-MD) placed at a distance of 15 cm, 14 cm and 8 cm from the SiPM respectively. The SiPM was biased with a negative voltage applied to the anode, while the cathode was connected to ground. The signal was collected from the cathode on a 50 Ω load resistor and amplified of a factor 10 with a voltage amplifier [58]. The SiPM was soldered on the amplifier board in order to remove the pick-up noise typical of high frequency fast amplifiers. The amplified signal was read out with the digital oscilloscope (TEKTRONIX DPO71604B) at

a sampling frequency of 50 GS/s and with a bandwidth of 16 GHz. The synchronization output of the pulsed diode laser driver was used as trigger signal. The waveforms were stored in a computer and analyzed with digital signal processing methods.

The integral of the waveform was calculated summing the measured voltage amplitudes in the time window of 80 ns, 100 ns and 120 ns for the 1 mm^2, 4 mm^2 and 9 mm^2 SiPM respectively. The number of photons emitted by the light source and detected in the SiPM follows the statistical distribution of a multi-photon state. The following selection criteria were applied in order to identify single photon events:

1) The waveform integral is within 1 σ from the average value of the integral of a single photon signal.
2) The maximum signal amplitude calculated in the range (0, 30) ns is within 10 mV of the amplitude of a single photon signal.

The arrival time of a triggered signal was defined at a threshold of half the amplitude of the signal corresponding to a single detected photon. The crossing time was measured using a linear interpolation method between the two points immediately below and above the voltage threshold on the rising edge of the signal.

The light emission of the picosecond fast pulsed diode laser has a typical timing structure. According to the theory of light emitting silicon devices [59], a fast high intensity component with a width of $\sigma_1 = 50$ ps (FWHM) is followed after 200 ps by a slow low intensity delayed component with a width of 80 ps (FWHM) and with an exponential tail. We fitted the measured arrival time of the single photons Δt with the model:

$$
\begin{aligned}
\Delta t[\text{ns}] = & f_1 \frac{1}{\sqrt{2\pi \left(\sigma_1^2 + \sigma_{sipm}^2\right)}} \exp\left[-\frac{(t - \mu_1)^2}{\sigma_1^2 + \sigma_{sipm}^2}\right] \\
& + f_2 \int \frac{1}{\sqrt{2\pi \left(\sigma_2^2 + \sigma_{sipm}^2\right)}} \exp\left[-\frac{(t - t' - \mu_1 - 0.2)^2}{\sigma_2^2 + \sigma_{sipm}^2}\right] \\
& \times \exp[-\tau t']dt'
\end{aligned}
\tag{1}
$$

where μ_1 is the arrival time of the fast laser component, σ_{sipm} is the intrinsic time resolution of the SiPM and $f_1 = 1 - f_2$.

The single photon time resolution *SPTR* was estimated as $2.35 \times \sigma_{sipm}$. The dependence of the single photon time resolution on the number of microcells N_{cells} in the tested SiPM was fitted with the function:

$$
SPTR = \sqrt{\alpha N_{cells} + \beta N_{cells}^2}
\tag{2}
$$

The first term represents the statistical fluctuation due to the intrinsic difference of the microcells, the second term models the additional confusion error introduced by dark count rate signals misidentified as detected single photons.
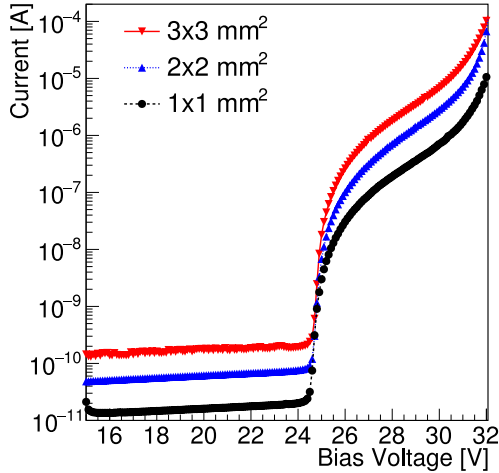
III. RESULTS
A. CURRENT-VOLTAGE CHARACTERIZATION
The measured current-voltage curve of the 1 mm^2, 4 mm^2 and 9 mm^2 SiPMs at a temperature of 20° averaged above

TABLE 1. **Dark current level and capacitance scale linearly with the area of the SiPM.**
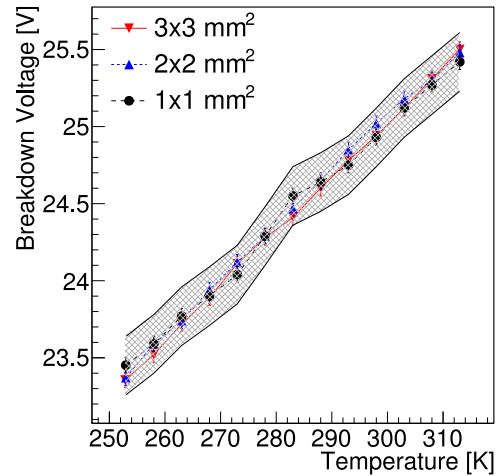
SiPM area [mm^2]	Dark current [pA]	Capacitance [pF]
1	24.1	66.9
4	84	270.2
9	213	554.0

FIGURE 3. **Current-voltage curves measured for the reverse-biased 1 × 1 (black circles), 2 × 2 (blue rectangles) and 3 × 3 (red triangles) SiPMs at a temperature of 20°.**

FIGURE 4. **Temperature dependence of the breakdown voltage of the 1 × 1 (black circles), 2 × 2 (blue rectangles) and 3 × 3 (red triangles) SiPMs. The gray band represents the total variation (FWHM) across the 120 samples considered in this paper.**

TABLE 2. **Dark count rate and cross talk for the different SiPMs at a reference Overvoltage of 2.5 V.**

SiPM area [mm^2]	Dark count rate [KHz/mm^2]	Cross talk %
1	166.2 ± 0.4	5.3 ± 0.4
4	188.6 ± 0.2	5.8 ± 0.2
9	232.2 ± 0.1	5.7 ± 0.3

120 samples is shown in Fig. 3. The average breakdown voltage is 24.89 V with a variation of 0.44 V (FWHM). The punch-through voltage is 32.59 V with a variation of 0.50 V (FWHM). The dark current level in the proportional response region is reported in the second column of Table 1. Its value scales linearly with the total area of the SiPM. The dark current level is an important quality control of the SiPM mass production. In fact, as the number of thermally generated pairs increases linearly with the area of the device, at a constant temperature, the dark current level is expected to follow a similar linear behavior and is easily predictable. The measurement of the dark current is performed with an accuracy of few pA and any significant deviation may indicate a non-uniformity of the distribution of impurities during the production stage.

The temperature dependence of the breakdown voltage is shown in Fig. 4 for the 1 mm^2, 4 mm^2 and 9 mm^2 SiPMs. The temperature coefficient extracted from the linear behavior of the data points is (35.17 ± 0.07) mV/K and is independent from the area of the device.

The measured capacitance of the three devices is reported in the third column of Table 1. The variation of the capacitance (FWHM) in the 120 measured samples is 1.08 pF, 4.5 pF and 12.5 pF for the 1 mm^2, 4 mm^2 and 9 mm^2 SiPMs respectively. The value of the capacitance scales linearly with the total area of the device. The capacitance of the single 50 × 50 μm^2 microcell at breakdown is estimated as 170 fF with a variation of approximately 3 fF (FWHM) across the 120 measured samples.

B. DARK COUNT RATE AND CROSS TALK

The measured average dependence of the dark count rate on the voltage threshold is shown in Fig. 5a at a overvoltage ranging from 1 V to 3 V. The plateaux corresponding to the increasing number of coincident pulses from independent cells within the observation time window are well visible in the 1 mm^2 and 4 mm^2 SiPMs and moderately visible in the 9 mm^2 SiPM.

The dark count rate at the first plateau ranges approximately between 60 kHz/mm^2 and 250 kHz/mm^2 at 1 V and 3 V overvoltage respectively. The fluctuation across the 120 measured samples ranges approximately between 5 kHz/mm^2 and 20 kHz/mm^2 (FWHM).

The dark count rate of the three devices measured at 2.5 V overvoltage is shown in the second column of Table 2. At first glance the measured values may indicate that the dark rate is not scaling linearly with the area. However, the observed discrepancy between the different measurements is consistent with the variation of 10% (FWHM) due to the intrinsic properties of the process used for the fabrication.

The cross talk of the three devices plotted versus the bias voltage is shown in Fig. 6. Its value is always below 10%. The cross talk of the three devices measured at 2.5 V overvoltage is shown in the third column of Table 2. The geometrical arrangement of the microcells is identical in the three devices and the cross talk is not affected by the area of the SiPMs.
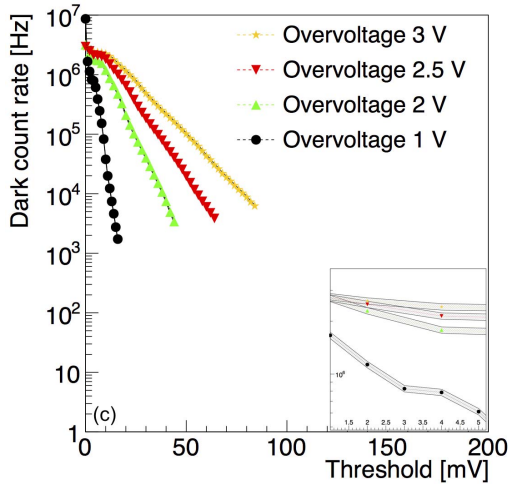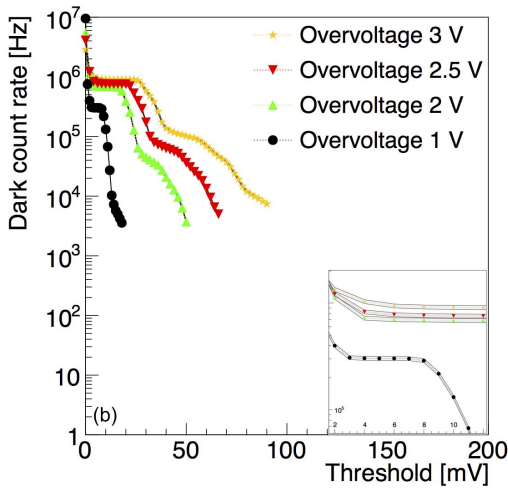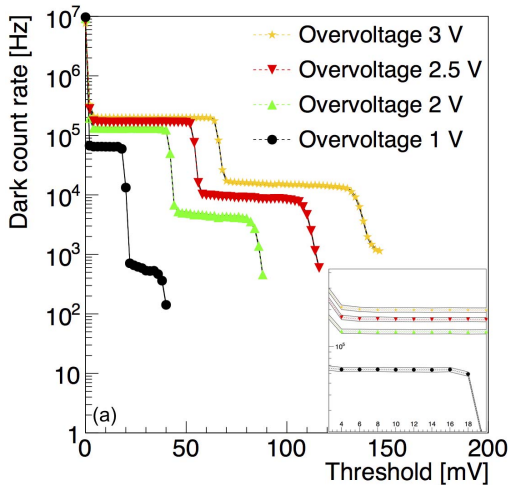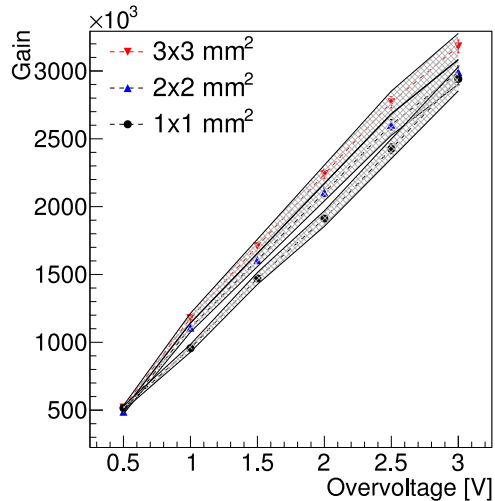
FIGURE 5. Dark count rate of the 1 × 1 (a), 2 × 2 (b) and 3 × 3 (c) SiPMs measured at different reverse bias voltage. The gray band represents the total variation (FWHM) across the 120 samples considered in this paper.

C. GAIN

The gain of the three SiPMs is shown in Fig. 7 as a function of the overvoltage. The gain at an overvoltage of 2.5 V is approximately 2.5×10^6. It increases linearly
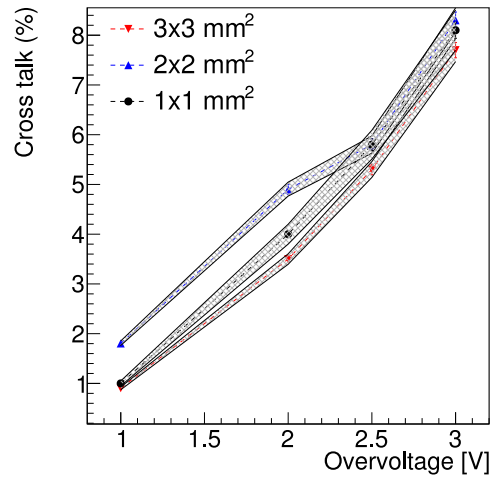
FIGURE 6. Cross talk plotted versus bias voltage for the 1 × 1 (black circles), 2 × 2 (blue rectangles) and 3 × 3 (red triangles) SiPMs. The gray band represents the total variation (FWHM) across the 120 samples considered in this paper.


FIGURE 7. Gain of the 1 × 1 (black circles), 2 × 2 (blue rectangles) and 3 × 3 (red triangles) SiPMs measured at different reverse bias voltage. The gray band represents the total variation (FWHM) across the 120 samples considered in this paper.

with the applied overvoltage, following the expected behavior of SiPMs [51]. The fluctuation across the 120 measured samples is approximately 5% (FWHM) for each sensor type.

D. PHOTON DETECTION EFFICIENCY

The photon detection efficiency of the 1 mm², 4 mm² and 9 mm² SiPMs at an overvoltage of 2.3 V is shown in Fig. 8. Only one curve is shown for the three device types, averaged over the 120 measured samples. It has a maximum of approximately 35% in response to photons with wavelength ranging between 420 nm and 440 nm. The photon detection efficiency depends on the structure of the microcell and on the geometrical configuration of the array. Thus there is no dependence on the area of the
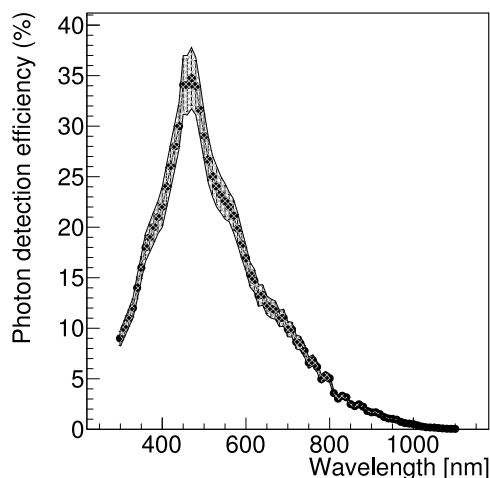
FIGURE 8. Photon detection efficiency of the 1 mm², 4 mm² and 9 mm² SiPMs at an overvoltage of 2.3 V. As the filling factor of the three SiPMs is identical, the photon detection efficiency is not dependent on the area of the sensor. The gray band represents the total variation (FWHM) across the 120 samples considered in this paper.
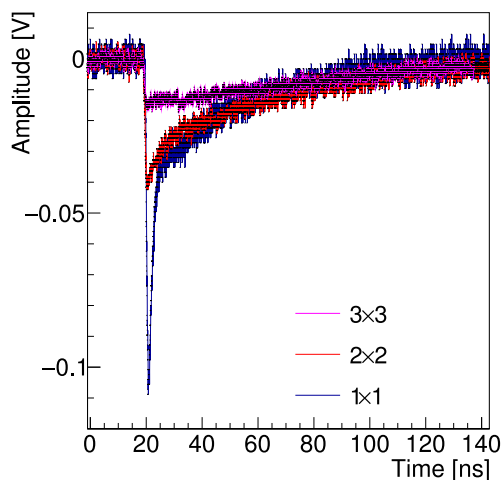
FIGURE 9. Signal corresponding to the detection of a single photon with the 1 × 1 (blue line), 2 × 2 (purple line) and 3 × 3 (red line) SiPMs.

three device types. The fluctuation across the 120 measured samples is approximately 2% (FWHM) for each sensor type.

E. SINGLE PHOTON TIME RESOLUTION

The signal corresponding to the detection of a single photon in the three devices is shown in Fig. 9 after 10× amplification. The 1 mm² device exhibits a single photon signal with amplitude of approximately 100 mV. The rising edge of the signal is exponential with a time constant of (234.0 ± 2.3) ps determined by the internal resistance of the microcell and the stray anode capacitance. The measurement of the time constant is limited by the bandwidth of the setup. The signal reaches its maximal amplitude when quenching occurs. After that, the falling edge is determined by the discharge of the internal microcell capacitance. The discharge has two contributions. A fast one has a decay time

of approximately (2.1 ± 0.2) ns and is due to the presence of a stray capacitance in parallel to the quenching resistance that allows to bypass the resistance itself. A slower one has a decay time of approximately (27.1 ± 0.1) ns and is determined by the quenching resistor and the anode stray capacitances.

We have shown in Section III-A that the total output capacitance increases with the area of the device. Consequently, the signal amplitude decreases in larger area SiPMs. The 4 mm² device exhibits a single photon signal with amplitude of approximately 40 mV. The rising edge of the signal is exponential with a time constant of (245.0 ± 3.5) ps, it does not show a significant deviation from the value measured with the 1 mm² SiPM and is limited by the bandwidth of the measurement system. After the quenching occurs, the fast decay component is less pronounced than in the 1 mm² SiPM and the slow decay component has a decay time of approximately (50.8 ± 0.2) ns. The 9 mm² device follows the trend observed in the 4 mm² SiPM, exhibiting a smaller single photon signal amplitude of approximately 15 mV, rising edge of approximately (240.0 ± 3.5) ps, absent fast decay component and slow decay component with decay time (78.2 ± 0.1) ns.

The integral of the signal corresponding to the detection of the light emitted by the fast pulsed diode laser is shown in Fig. 10a, 11a and 12a for the 1 mm², 4 mm² and 9 mm² SiPM respectively. The spectra measured with the 1 mm² and the 4 mm² SiPM are showing few well discriminated peaks, the first corresponding to the electronic noise pedestal, the second to one detected photon, the nth to $n-1$ detected photons. The spectrum measured with the 9 mm² SiPM is showing only two well-defined peaks corresponding to the electronic pedestal and to one detected photon. When more photons are detected, the larger tail of the signal falls outside the integration window and the range of the oscilloscope and do not allow a precise measurement of the total charge.

The single photon events, selected according to the criteria outlined in Section II-F, are represented by the red filled area in the histograms. The distribution of the arrival time corresponding to the selected single photon events is shown in Fig. 10b, 11b and 12b for the 1 mm², 4 mm² and 9 mm² SiPM respectively. The time spectrum is fitted with the function in Eq. (1). It is consistent with the timing structure of the emission of the light from the fast pulsed diode laser and shows two clear components with a distance of approximately 200 ps. The single photon time resolution (FWHM) is estimated as (77.97 ± 0.51) ps, (201.67 ± 0.98) ps and (282.28 ± 0.86) ps for the 1 mm², 4 mm² and 9 mm² SiPMs respectively. The fluctuation across the 120 measured samples is approximately 5% (FWHM) for each sensor type.

The dependence of the single photon time resolution of the SiPM on the number of microcells is shown in Fig. 13. The model is fitted with the function in Eq. (2). The resulting parameters are $\alpha = (17.74 \pm 0.21)$ ps² and
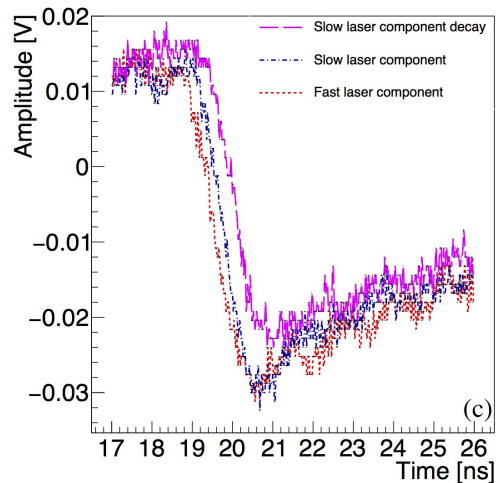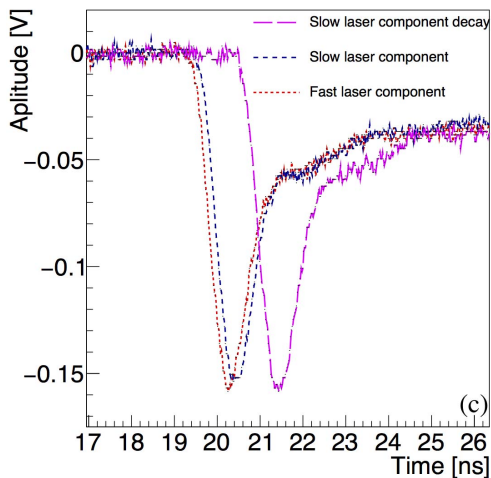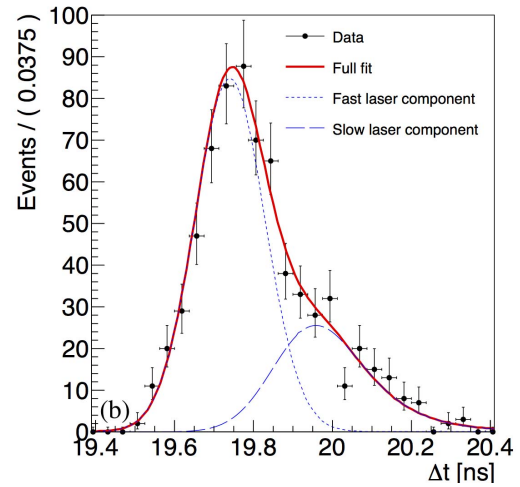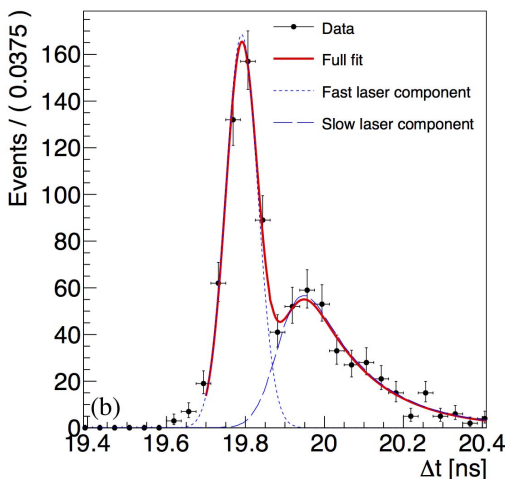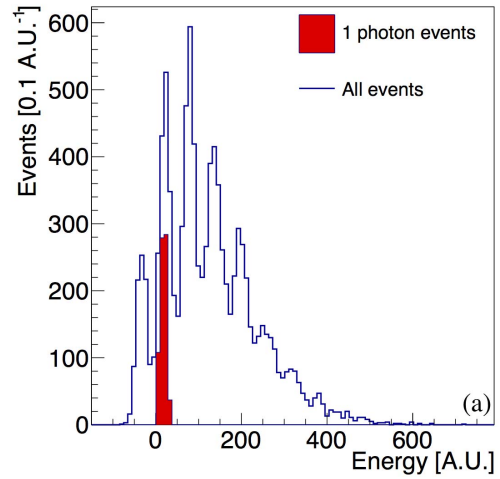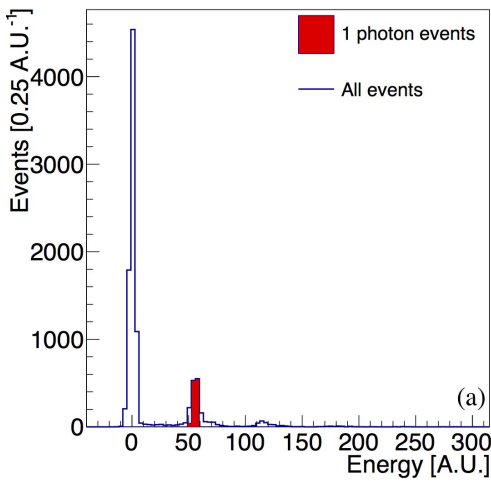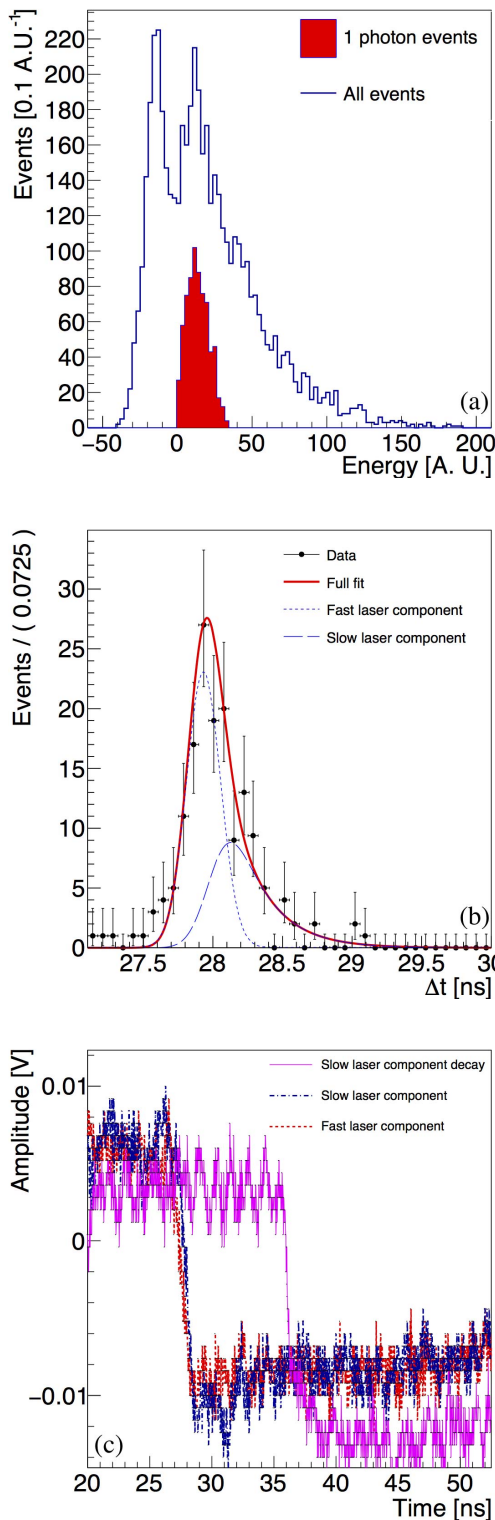
FIGURE 10. **1 × 1 SiPM:** Low photon flux and single photon event selection (a), single photon time resolution (b) and single photon signals corresponding to different fast laser pulses (c).

FIGURE 11. **2 × 2 SiPM:** Low photon flux and single photon event selection (a), single photon time resolution (b) and single photon signals corresponding to different fast laser pulses (c).

$\beta = (1.43 \pm 0.08) \times 10^{-3}$ ps^2. We observe that the confusion term (FWHM) is approximately (15.12 ± 0.01) ps for the 1 mm^2 SiPM and increases up to (136.12 ± 0.01) ps for the 9 mm^2 SiPM.
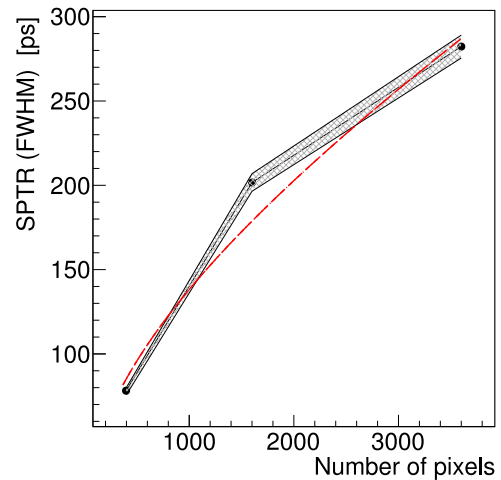
The timing structure of the light emitted from the fast diode laser allows to visualize the discrimination power of the SiPMs. By way of example, the leading edge of the signals corresponding to the components of the laser emission

FIGURE 13. Dependence of the single photon time resolution upon the number of pixels. The gray band represents the total variation (FWHM) across the 120 samples considered in this paper.

three components of the light emission better with respect to the 9 mm^2 device, due to the larger maximal amplitude and the better intrinsic single photon time resolution.

IV. DISCUSSION

The benchmarking of the experimental results needs to follow a twofold approach. On the one side, it is needed to benchmark against the mature available SiPMs, which are not always developed in standard CMOS technology but in dedicated lines with additional optimized masks. This first comparison allows us to understand how far is the standard CMOS process used in this work from the behavior of specifically optimized processes for good-performing commercial SiPM. On the other side, it is needed to benchmark against other experimental attempts of using standard CMOS processes for the production of SiPM. This second comparison allows us understanding how the chosen CMOS technology process performs with respect to other available ones.

A first set of parameters is not sensitive to the area of the device but is indicative of the quality of the produced SiPMs.

The breakdown voltage depends only on the doping profile of the microcells and does not depend on the area of the sensor [60]. The measured value is consistent with reported results. Breakdown voltages in the range from 18.9 V to 27.5 V are obtained in similar 0.35 μm CMOS technology nodes [26], [29], [34], [51]. Smaller scale CMOS processes report usually smaller breakdown voltages. By way of example, a breakdown voltage of 12 V was obtained in our previous studies at the 0.18 μm [35], [38] and in [6] CMOS node. This value depends on the high doping concentration of the standard CMOS wells at small scales, which ranges from 2×10^{17} cm^{-3} to 5×10^{17} cm^{-3}. The SiPM proposed in this paper has a structure very similar to the one in our previous publication [34], where a general Multi Project Wafer approach was used for the fabrication of the

FIGURE 12. 3 × 3 SiPM: Low photon flux and single photon event selection (a), single photon time resolution (b) and single photon signals corresponding to different fast laser pulses (c).

are shown in Fig. 10c, 11c and 12c for the 1 mm^2, 4 mm^2 and 9 mm^2 SiPM respectively. The signal corresponding to the single photon detection is stable in amplitude and shape. However, the 1 mm^2 and 4 mm^2 SiPMs discriminate the

prototype. Here a dedicated optimized engineering run is presented in preparation to the pilot production of the devices and the breakdown voltage is approximately 1 V smaller than in [34]. In comparison to commercial SiPMs obtained with custom technologies, the breakdown voltage of the proposed CMOS SiPMs is compatible with Ketek (25 V) [1], SensL (24.5 V) [2] and AdvanSid (26 V) [5]. It is lower than Hamamatsu (68 V) [3] and Excelitas (95 V) [4]. The variation of the breakdown voltage across wafers is one of the parameters for the verification of the stability of the production. The variation of the breakdown voltage of the proposed SiPMs is approximately 1.6% (FWHM) and is compatible with values obtained in commercial SiPMs.

When the temperature increases, the impact ionization coefficient decreases with a consequent increase of the breakdown voltage. The variation of the breakdown voltage with temperature is a critical parameter when evaluating the stability of the operation of the SiPM. For example, a temperature coefficient of 30 mV/K was obtained at a 0.35 μm CMOS node [51] and a better value as low as 17 mv/K was recently reported at a 0.15 μm scale [54]. With respect to custom technologies we observe a slightly stronger temperature dependence than SensL (21.5 mv/K) [2] and Advansid (26 mV) [5]. However, we observe a much weaker temperature dependence than Hamamatsu (60 mV/K) [3] and Excelitas (90 mV/K) [4].

The dark count rate of the CMOS SiPMs presented in this paper is found in agreement with our previous results in [34] and shows a clear improvement with respect to other devices developed with CMOS processes. A typical feature of SiPMs manufactured in CMOS technology is a higher dark count rate with respect to custom technology SiPMs, due to either STI or higher doping concentration. An increase of the dark count rate was observed, for example, in the study at 0.35 μm and 0.09 μm CMOS technology node [24], [47]. Dark count rate values as high as 20×10^3 kHz/mm^2 were observed in our previous publications at the 180 nm CMOS technology node [35], [38] and in [6]. The dark count rate obtained in this paper is two order of magnitudes lower than at smaller CMOS scales. Furthermore, it is three times lower than in a SiPM obtained with a similar 0.35 μm CMOS process [51]. Custom technologies are optimized to minimize the dark count rate. For example, a value as low as 50-60 kHZ/mm^2 is available at Hamamatsu [3] and 110 kHz/mm^2 at SensL [2]. However, SiPMs from Excelitas [4] and Advansid [5] exhibit a dark count rate as high as 300 kHz/mm^2 and 600 kHz/mm^2 respectively, thus larger than the CMOS SiPM proposed in this paper.

The cross talk depends on the distance between the microcells and other geometrical parameters of the layout. It does not depend on the area of the device. The obtained value is consistent both with CMOS SiPMs fabricated in similar scaled CMOS technology [51] and with SiPMs in commercial custom technologies [2].

As the cross talk, the photon detection efficiency is not dependent on the area of the device. PDE values ranging

from 1.3% to 25% were measured for SiPMs designed at 0.18 μm [6], [35], 0.35 μm [26] and 0.8 μm [19]. The PDE of the manufactured device is thus better than what reported in other CMOS technologies and is compatible with SiPMs obtained with a similar 0.35 μm CMOS process [51]. Commercial custom technologies were optimized to allow a better PDE and offer a slightly better photon detection efficiency up to 40% in the 420 nm-440 nm spectral range [2], [3], [5].

The parameters affected by the area of the SiPM are mainly related to the total output capacitance of the microcell. One of the most significant limitations to the design of large area SiPMs is that the capacitance scales with the total area of the device and the resulting output signal is smoothed under the noise level of the sensor. It is thus needed to keep the total capacitance of a microcell as low as possible. With respect to sensors obtained in CMOS technology, the proposed SiPMs have a smaller capacitance. By way of example, a microcell capacitance of approximately 300 fF was obtained for a 1 mm^2 SiPM manufactured at the 0.35 μm node with 50×50 μm^2 cells [51]. With respect to custom commercial technologies, the proposed CMOS SiPM has larger capacitance than Hamamatsu MPPC. In fact the custom technology developed by Hamamatsu allows a typical terminal capacitance of 60 pF, 140 pF and 320 pF for the 1 mm^2, 4 mm^2 and 9 mm^2 devices respectively. Such a small capacitance allows to scale the Hamamatsu technology up to an area of 36 mm^2 [3]. However, the proposed CMOS SiPM has $2\times$ smaller capacitance than the SensL-C series SiPM, which exhibits a typical terminal capacitance of 110 pF and 920 pF for the 1 mm^2, 9 mm^2 devices respectively [2].

An higher pixel capacitance implies higher gain. Our results are consistent with CMOS SiPMs fabricated in similar scaled CMOS technology [51]. Our gain is still higher than most commercial SiPMs, except for SensL that reports a gain of 6×10^6 at 2.5 V excess voltage [2].

A larger gain is not always an advantage, as it is due to a larger capacitance and affects the timing structure of the signal. For example single photon detection structures obtained at the 0.18 μm CMOS technology node exhibits a decay time of approximately 60 ns [38]. However, commercial SiPMs with higher capacitance and gain exhibit longer decay times up to 300 ns for large area of 9 mm^2 [2]. The introduction of an output derivative circuit [2] or in-chip trans-impedence amplifiers [53] can improve the signal to noise ratio. The CMOS SiPMs proposed in this paper show a single photon signal with a sizable amplitude and decay tail lower than most of the commercial SiPMs for a total area up to 9 mm^2.

The timing structure of the single photon signal has a clear impact on the timing properties of the SiPM. Recently, a single photon detection structure consisting of an array of 5×5 SPAD structures with 10 μm diameter obtained at the 0.15 μm CMOS node was reported [54]. A single photon time resolution of 52 ps (FWHM) was measured by

disentangling the different components of the fast pulsed diode laser. When the area of the array increases, two problems occur and contribute to the degradation of the single photon time resolution. The first is the non-uniformity of the response of single cells, due to the different output capacitance at different positions. The second is the increase of dark count rate pulses, which are misidentified as single photons. A comparative study of the single photon time resolution of commercial SiPMs was recently performed [55]. Devices with 1 mm² area exhibited a single photon time resolution as low as approximately 100 ps (Advansid, Hamamatsu). However, the result worsens for 9 mm² SiPMs up to approximately 200 ps (Hamamatsu) and 250 ps (SensL). The single photon time resolution of the CMOS SiPMs proposed in this paper scales with the area of the device preserving a value that follows the trend of commercial SiPMs obtained in custom technology.

V. CONCLUSION

We reported the design and characterization of CMOS SiPMs with area up to 9 mm². It is the first time to our knowledge that a SiPM obtained in a CMOS technology node is proposed with such large area. The measurement allowed us both to understand the general behavior of the device and to study these parameters that are scaling with the area of the device.

Dark count rate, cross talk, photon detection efficiency at 420 nm, gain at 2.5 V overvoltage and breakdown voltage temperature coefficient have a value of 180 kHz/mm², 10%, 35%, 2.5×10^6 and 35 mV/K respectively and are following the trend of most SiPMs obtained with CMOS and custom technology processes.

The most sensitive parameter for large area SiPMs is the total output capacitance, which affects the decay time of the single photon signal and the single photon time resolution of the device. We obtain a capacitance of 66.9 pF, 270.2 pF and 554.0 pF, a decay time of (27.1 ± 0.1) ns, (50.8 ± 0.1) ns and (78.2 ± 0.1) ns and a SPTR of (77.97 ± 0.51) ps, (201.67 ± 0.98) ps and (282.28 ± 0.86) ps for the 1 mm², 4 mm² and 9 mm² SiPMs respectively. The obtained CMOS SiPM hence shows a good compromise among capacitance, gain, and timing. The obtained parameters are competitive with SiPMs in custom technology processes.

The spread of the measured parameters across 120 samples obtained at different dices and wafers shows that the used 0.35 μm process reached a stability comparable to custom technologies. The 0.35 μm technology line and the sensor design are mature for the development of integrated electronics within the chip to the aim of a digital device.

REFERENCES

[1] *Ketek PM1150NT*. Accessed: Aug. 2018. [Online]. Available: www.ketek.ne

[2] *SensL C Series 10050*. Accessed: Aug. 2018. [Online]. Available: www.SensL.com

[3] *Hamamatsu MPPC S12571-50c*. Accessed: Aug. 2018. [Online]. Available: www.hamamatsu.com

[4] *Excelitas C30742-11-050*. Accessed: Aug. 2018. [Online]. Available: www.excelitas.com

[5] *AdvanSiD ASD-RGB1S-P*. Accessed: Aug. 2018. [Online]. Available: www.avansid.com

[6] I. Vornicu, F. N. Bandi, R. Carmona-Galán, and Á. Rodríguez-Vázquez, "A CMOS digital SiPM with focal-plane light-spot statistics for DOI computation," *IEEE Sensors J.*, vol. 17, no. 3, pp. 632–643, Feb. 2017, doi: 10.1109/JSEN.2016.2632200.

[7] P. Fischer *et al.*, "A dense SPAD array with full frame readout and fast cluster position reconstruction," in *Proc. IEEE NSS MIC Conf.*, Seattle, WA, USA, 2014, pp. 8–15. [Online]. Available: https://doi.org/10.1186/2197-7364-2-S1-A3

[8] K. Xu, "Integrated silicon directly modulated light source using p-well in standard CMOS technology," *IEEE Sensors J.*, vol. 16, no. 16, pp. 6184–6191, Aug. 2016, doi: 10.1109/JSEN.2016.2582840.

[9] K. Xu *et al.*, "Silicon light-emitting device in standard CMOS technology," in *Proc. Optoelectron. Device Integr.*, Wuhan, China, Jun. 2015, Paper OT1C.3. [Online]. Available: https://doi.org/10.1364/OEDI.2015.OT1C.3

[10] S. Gnecchi, S. Bellis, D. Herbert, and C. Jackson, "First results from CMOS-integrated SPAD and SiPM," in *Proc. IEEE NSS MIC Conf.*, Atlanta, GA, USA, 2017, pp. 1–4. [Online]. Available: http://sensl.com/downloads/irp/A_IEEE17_First%20Results_CMOS_SPAD_V1p0.pdf

[11] C. Niclass, A. Rochas, P.-A. Besse, and E. Charbon, "Toward a 3-D camera based on single photon avalanche diodes," *IEEE J. Sel. Topics Quantum Electron.*, vol. 10, no. 4, pp. 796–802, Jul./Aug. 2004, doi: 10.1109/JSTQE.2004.833886.

[12] A. Rochas *et al.*, "First fully integrated 2-D array of single-photon detectors in standard CMOS technology," *IEEE Photon. Technol. Lett.*, vol. 15, no. 7, pp. 963–965, Jul. 2003, doi: 10.1109/LPT.2003.813387.

[13] S. Tisa, F. Zappa, and I. Labanca, "On-chip detection and counting of single-photons," in *IEEE Int. Electron Devices Meeting IEDM Tech. Dig.*, vol. 2005, Dec. 2005, pp. 815–818, doi: 10.1109/IEDM.2005.1609480.

[14] D. Stoppa *et al.*, "A CMOS 3-D imager based on single photon avalanche diode," *IEEE Trans. Circuits Syst. I, Reg. Papers*, vol. 54, no. 1, pp. 4–12. Jan. 2007, doi: 10.1109/TCSI.2006.888679.

[15] C. Niclass, A. Rochas, P.-A. Besse, and E. Charbon, "Design and characterization of a CMOS 3-D image sensor based on single photon avalanche diodes," *IEEE J. Solid-State Circuits*, vol. 40, no. 9, pp. 1847–1854, Sep. 2005, doi: 10.1109/JSSC.2005.848173.

[16] D. Stoppa *et al.*, "A single-photon-avalanche-diode 3D imager," in *Proc. 31st Eur. Solid-State Circuits Conf. ESSCIRC*, Grenoble, France, Sep. 2005, pp. 487–490, doi: 10.1109/ESSCIR.2005.1541666.

[17] A. Rochas *et al.*, "Single photon detector fabricated in a complementary metal-oxide-semiconductor high-voltage technology," *Rev. Sci. Instrum.*, vol. 74, no. 7, pp. 3263–3270, Jul. 2003, doi: 10.1063/1.1584083.

[18] F. Nolet *et al.*, "A 2D proof of principle towards a 3D digital SiPM in HV CMOS with low output capacitance," *IEEE Trans. Nucl. Sci.*, vol. 63, no. 4, pp. 2293–2299, Aug. 2016, doi: 10.1109/TNS.2016.2582686.

[19] B.-L. Bérubé *et al.*, "Implementation study of single photon avalanche diodes (SPAD) in 0.8 μm HV CMOS technology," *IEEE Trans. Nucl. Sci.*, vol. 62, no. 3, pp. 710–718, Jun. 2005, doi: 10.1109/TNS.2015.2424852.

[20] L. Pancheri and D. Stoppa, "Low-noise CMOS single-photon avalanche diodes with 32 ns dead time," in *Proc. 37th Eur. Solid-State Device Res. Conf. ESSDERC*, Munich, Germany, Sep. 2007, pp. 362–365, doi: 10.1109/ESSDERC.2007.4430953.

[21] M. H. U. Habib and N. Mcfarlane, "A perimeter gated single photon avalanche diode based silicon photomultiplier as optical detector," in *Proc. IEEE 58th Int. Midwest Symp. Circuits Syst. (MWSCAS)*, Fort Collins, CO, USA, Aug. 2015, pp. 1–4, doi: 10.1109/MWSCAS.2015.7282084.

[22] J. Gu, M. H. U. Habib, and N. Mcfarlane, "Perimeter-gated single-photon avalanche diodes: An information theoretic assessment," *IEEE Photon. Technol. Lett.*, vol. 28, no. 6, pp. 701–704, Mar. 2016, doi: 10.1109/LPT.2015.2505241.

[23] K. Jradi, D. Pellion, and D. Ginhac, "Design, characterization and analysis of a 0.35 μm CMOS SPAD," *Sensors*, vol. 14, no. 12, pp. 22773–22784, Dec. 2014, doi: 10.3390/s141222773.

[24] E. Vilella and A. Diéguez, "A gated single-photon avalanche diode array fabricated in a conventional CMOS process for triggered systems," *Sensors Actuators A Phys.*, vol. 186, pp. 163–168, Oct. 2012. [Online]. Available: https://doi.org/10.1016/j.sna.2012.01.019

[25] I. Nissinen *et al.*, "A sub-ns time-gated CMOS single photon avalanche diode detector for Raman spectroscopy," in *Proc. 41st Eur. Solid-State Device Res. Conf.*, Helsinki, Finland, Sep. 2011, pp. 375–378. [Online]. Available: https://doi.org/10.1109/ESSDERC.2011.6044156

[26] E. Vilella, O. Alonso, A. Montiel, A. Vilá, and A. Diéguez, "A low-noise time-gated single-photon detector in a HV-CMOS technology for triggered imaging," *Sensors Actuators A Phys.*, vol. 201, pp. 342–351, Oct. 2013, doi: 10.1016/j.sna.2013.08.006.

[27] A. Arbat *et al.*, "High voltage vs. high integration: A comparison between CMOS technologies for SPAD cameras," in *Proc. SPIE*, vol. 7780, Aug. 2010, Art. no. 77801G, doi: 10.1117/12.860482.

[28] D. Stoppa, D. Mosconi, L. Pancheri, and L. Gonzo, "Single-photon avalanche diode CMOS sensor for time-resolved fluorescence measurements," *IEEE Sensors J.*, vol. 9, no. 9, pp. 1084–1090, Sep. 2009, doi: 10.1109/JSEN.2009.2025581.

[29] C. Niclass, C. Favi, T. Kluter, F. Monnier, and E. Charbon, "Single-photon synchronous detection," *IEEE J. Solid-State Circuits*, vol. 44, no. 7, pp. 1977–1989, Jul. 2009, doi: 10.1109/JSSC.2009.2021920.

[30] S. Tisa, F. Guerrieri, A. Tosi, and F. Zappa, "100 kframe/s 8 bit monolithic single-photon imagers," in *Proc. 38th Eur. Solid-State Device Res. Conf.*, Edinburgh, U.K., Sep. 2008, pp. 274–277, doi: 10.1109/ESSDERC.2008.4681751.

[31] S. Tisa, F. Guerrieri, and F. Zappa, "Variable-load quenching circuit for single-photon avalanche diodes," *Opt. Exp.* vol. 16, no. 3, pp. 2232–2244, Feb. 2008, doi: 10.1364/OE.16.002232.

[32] C. Niclass, C. Favi, T. Kluter, M. Gersbach, and E. Charbon, "A 128×128 single-photon image sensor with column-level 10-bit time-to-digital converter array," *IEEE J. Solid-State Circuits*, vol. 43, no. 12, pp. 2977–2989, Dec. 2008, doi: 10.1109/JSSC.2008.2006445.

[33] C. Niclass, M. Sergio, and E. Charbon, "A single photon avalanche diode array fabricated in 0.35 μm CMOS and based on an event-driven readout for TCSPC experiments," in *Proc. SPIE*, vol. 6372, Nov. 2006, Art. no. 63720S, doi: 10.1117/12.685974.

[34] N. D'Ascenzo *et al.*, "Design and characterization of a silicon photomultiplier in 0.35 μm CMOS," *IEEE J. Electron. Dev. Soc.*, vol. 6, pp. 74–80, Nov. 2017, doi: 10.1109/JEDS.2017.2771145.

[35] N. D'Ascenzo, Z. Xi, Q. Xie, "Application of CMOS technology to silicon photomultiplier sensors," *Sensors*, vol. 17, no. 10, p. 2204, Sep. 2017, doi: 10.3390/s17102204.

[36] H. Finkelstein, M. J. Hsu, and S. C. Esener, "STI-bounded single-photon avalanche diode in a deep-submicrometer CMOS technology," *IEEE Electron Device Lett.*, vol. 27, no. 11, pp. 887–889, Nov. 2006, doi: 10.1109/LED.2006.883560.

[37] N. Faramarzpour, M. J. Deen, S. Shirani, and Q. Fang, "Fully integrated single photon avalanche diode detector in standard CMOS 0.18-μ m technology," *IEEE Trans. Electron Devices*, vol. 55, no. 3, pp. 760–767, Mar. 2008, doi: 10.1109/TED.2007.914839.

[38] N. D'Ascenzo and Q. Xie, "Possible layout solutions for the improvement of the dark rate of geiger mode avalanche structures in the GLOBALFOUNDRIES BCDLITE 0.18 μm CMOS technology," *J. Instrum.*, vol. 13, Apr. 2018, Art. no. T04007. [Online]. Available: https://doi.org/10.1088/1748-0221/13/04/T04007

[39] L. Pancheri and D. Stoppa, "Low-noise single photon avalanche diodes in 0.15 μm CMOS technology," in *Proc. Eur. Solid-State Device Res. Conf. (ESSDERC)*, Helsinki, Finland, Sep. 2011, pp. 179–182, doi: 10.1109/ESSDERC.2011.6044205.

[40] J. A. Richardson, L. A. Grant, and R. K. Henderson, "Low dark count single-photon avalanche diode structure compatible with standard nanometer scale CMOS technology," *IEEE Photon. Technol. Lett.*, vol. 21, no. 14, pp. 1020–1022, Jul. 2009, doi: 10.1109/LPT.2009.2022059.

[41] M. Gersbach *et al.*, "A time-resolved, low-noise single-photon image sensor fabricated in deep-submicron CMOS technology," *IEEE J. Solid-State Circuits*, vol. 47, no. 6, pp. 1394–1407, Jun. 2012, doi: 10.1109/JSSC.2012.2188466.

[42] R. K. Henderson, J. Richardson, and L. Grant, "Reduction of band-to-band tunneling in deep-submicron CMOS single photon avalanche photodiodes," in *Proc. Int. Image Sensor Workshop*, Bergen, Norway, Jun. 2009, pp. 26–28.

[43] C. Niclass, M. Gersbach, R. Henderson, L. Grant, and E. Charbon, "A single photon avalanche diode implemented in 130-nm CMOS technology," *IEEE J. Sel. Topics Quantum Electron.*, vol. 13, no. 4, pp. 863–869, Jul./Aug. 2007. doi: 10.1109/JSTQE.2007.903854.

[44] A. Arbat, "Towards a froward tracker detector based on Geiger mode avalanche photodiodes for future linear colliders," Ph.D. dissertation, Dept. Electron., Univ. Barcelona, Barcelona, Spain, 2010.

[45] E. Vilella, O. Alonso, and A. Diéguez, "3D integration of geiger-mode avalanche photodiodes aimed to very high fill-factor pixels for future linear colliders," *Nucl. Instrum. Methods Phys. Res. A Accelerators Spectrom. Detect. Assoc. Equip.*, vol. 731, pp. 103–108, Dec. 2013. [Online]. Available: https://doi.org/10.1016/j.nima.2013.05.022

[46] M. A. Karami, M. Gersbach, H.-J. Yoon, and E. Charbon, "A new single-photon avalanche diode in 90nm standard CMOS technology," *Opt. Exp.* vol. 18, no. 21, pp. 22158–22166, Aug. 2010. doi: 10.1117/12.859435.

[47] E. A. G. Webster, J. A. Richardson, L. A. Grant, D. Renshaw, and R. K. Henderson, "A single-photon avalanche diode in 90-nm CMOS imaging technology with 44% photon detection efficiency at 690 nm," *IEEE Electron Device Lett.*, vol. 33, no. 5, pp. 694–696, May 2012. doi: 10.1109/LED.2012.2187420.

[48] K. Xu *et al.*, "Light emission from a poly-silicon device with carrier injection engineering," *Mater. Sci. Eng. B*, vol. 231, pp. 28–31, May 2018. [Online]. Available: https://doi.org/10.1016/j.mseb.2018.07.002

[49] D. Marris, E. Cassan, and L. Vivien, "Response time analysis of *SiGe/Si* modulation-doped multiple-quantum-well structures for optical modulation," *J. Appl. Phys.*, vol. 96, no. 11, pp. 6109–6111, Nov. 2004. [Online]. Available: https://doi.org/10.1063/1.1806995

[50] F. M. D. Rocca *et al.*, "Real-time fluorescence lifetime actuation for cell sorting using a CMOS SPAD silicon photomultiplier," *Opt. Lett.*, vol. 41, no. 4, pp. 673–676, Feb. 2016, doi: 10.1364/OL.41.000673.

[51] Y. Zou *et al.*, "Planar CMOS analog SiPMs: Design, modeling, and characterization," *J. Mod. Opt.*, vol. 62, no. 20, pp. 1693–1702, May 2015, doi: 10.1080/09500340.2015.1049572.

[52] B.-L. Bérubé *et al.*, "Implementation study of single photon avalanche diodes (SPAD) in 0.8 μm HV CMOS technology," *IEEE Trans. Nucl. Sci.*, vol. 62, no. 3, pp. 710–718, Jun. 2015, doi: 10.1109/TNS.2015.2424852.

[53] A. Schwinger, W. Brockherde, B. J. Hostickaa, and H. Vogt, "CMOS SiPM with integrated amplifier," in *Proc. SPIE*, vol. 10100, Feb. 2017, Art. no. 101001A. [Online]. Available: https://doi.org/10.1117/12.2252516

[54] H. Xu, L. Pancheri, G. D. Betta, and D. Stoppa, "Design and characterization of a p+/n-well SPAD array in 150nm CMOS process," *Opt. Exp.*, vol. 25, no. 11, pp. 12765–12778, May 2017. [Online]. Available: https://doi.org/10.1364/OE.25.012765

[55] M. V. Nemallapudi, S. Gundacker, P. Lecoq, and E. Auray, "Single photon time resolution of state of the art SiPMs," *J. Instrum.*, vol. 11, Oct. 2016, Art. no. P10016, doi: 10.1088/1748-0221/11/10/P10016.

[56] C. J. Thompson *et al.*, "Measurement of energy and timing resolution of very highly pixellated LYSO crystal blocks with multiplexed SiPM readout for use in a small animal PET/MR insert," in *Proc. IEEE Nucl. Sci. Symp. Med. Imag. Conf. (NSS/MIC)*, 2013, pp. 1–5, doi: 10.1109/NSSMIC.2013.6829134.

[57] "MPPC Module for PET," Technical Note, Hamamtsu, Iwata, Japan, 2017, [Online]. Available: https://www.hamamatsu.com/resources/pdf/ssd/pet_module_kacc9009e.pdf

[58] *MINICIRCUITS*. Accessed: Dec. 1, 2018. [Online]. Available: www.minicircuits.com

[59] K. Xu, "Monolithically integrated Si gate-controlled light-emitting device: Science and properties," *J. Opt.*, vol. 20, no. 2, pp. 024014–024022, Jan. 2018. [Online]. Available: https://doi.org/10.1088/2040-8986/aaa2b7

[60] A. S. Grove, O. Leistiko, and W. W. Hooper, "Effect of surface fields on the breakdown voltage of planar silicon p-n junctions," *IEEE Trans. Electron Devices*, vol. 14, no. 3, pp. 157–162, Mar. 1967, doi: 10.1109/T-ED.1967.15916.

XIAO LIANG received the B.S. degree in medicine from Fudan University in 2011. She is currently pursuing the Doctoral degree with PETLab@HUST. Her current research interests focus on the CMOS silicon photomultipliers and their application to the design of digital small animal PET/CT scanners.

STEFAN DREINER received the Diploma degree in physics from University GHS Essen, Essen, Germany, in 1996 and the Ph.D. degree in physics from the University of Münster, Münster, Germany, in 2002. He is the Manager of the Semiconductor Systems for Harsh Environment Group, Fraunhofer Institute of Microelectronic Circuits and Systems (IMS), Duisburg, Germany. He was a Post-Doctoral Fellow with the University of Dortmund, Dortmund, Germany. Since 2005, he has been with Fraunhofer IMS Institute.

NICOLA D'ASCENZO received the B.Sc. degree in physics and the M.S. degree in applied physics from the University of Pisa in 2003 and 2005, respectively, and the Ph.D. degree in natural sciences from the Physics Department, University of Hamburg. He is currently a Full Professor with the Department of Biomedical Engineering, Huazhong University of Science and Technology. His research focuses on physics and optoelectronics technologies for the development of multivoltage th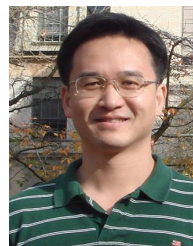reshold enabled photodetectors, to build new generation radiation imaging systems for applications to both high-energy physics and nuclear medicine. His research activities range from the physical modeling of high energy and medical physics phenomena and the related computational physics aspects in high performance computing, to the technological aspects of the sensor development and the design of full imaging systems.

ANDREI SCHMIDT received the Dipl.-Ing. degree in electrical engineering from the University of Ulm, Ulm, Germany, in 2010 and the Ph.D. degree from the University Duisburg-Essen, Duisburg, Germany, in 2016. He is currently with the Fraunhofer Institute for Microelectronic Circuits and Systems IMS, Duisburg. His current research interests include characterization, modeling, and TCAD simulation of single-photon avalanche diodes.

WERNER BROCKHERDE received the Dipl.-Ing. degree in electrical engineering from the University of Dortmund, Germany, in 1982. He is heading the department Optical Sensor Systems and also the business field CMOS image sensors with the Fraunhofer Institute of Microelectronic Circuits and Systems (IMS), Duisburg, Germany. From 1982 to 1984, he was with the Lehrstuhl Bauelemente der Elektrotechnik, Department of Electrical Engineering, University of Dortmund, researching in the field of analog and digital MOS integrated circuits design. In 1985, he joined Fraunhofer IMS. He has authored and co-authored over 100 scientific papers and over 20 patents. His scientific interests include CMOS imager design techniques and low-noise CMOS circuits. He has been serving as a member of the Technical Program Committee of the European Solid-State Circuits Conference since 1993.

QINGGUO XIE received the B.S. degree in industrial automation from the Huazhong University of Science and Technology (HUST) in 1994, the M.S. degree in industrial automation from the Dalian University of Technology in 1997, and the Ph.D. degree in electric engineering from HUST in 2001, where he is currently a Distinguished Professor with the Department of Biomedical Engineering and an Adjunct Professor with the Wuhan National Laboratory for Optoelectronics. He founded PETLab@HUST in 2001 and the laboratory focuses on working in physics, information, and optoelectronics technologies for the development of all-digital PET instrumentation and its biomedical applications, ranging from the development of key components, such as new photodetectors for building PET detectors, the development of multivoltage threshold enabled all-digital PET detector technologies for imaging to the building of complete imaging systems for specific biological or medical applications. His team is also exploring new applications of molecular imaging technologies for both preclinical and clinical researches and trials in cancers and brain disorders, and the development and validation for new drugs and therapeutic approaches.